Chromatin structure-dependent histone incorporation revealed by a genome-wide deposition assay

Hiroaki Tachiwana[a], Mariko Dacher[b], Kazumitsu Maehara[d], Akihito Harada[d], Yasuyuki Ohkawa[d], Hiroshi Kimura[c], Hitoshi Kurumizaka[b], Noriko Saitoh[a]

[a]Division of Cancer Biology, The Cancer Institute of Japanese Foundation for Cancer Research, Tokyo 135-8550, Japan; [b]Laboratory of Chromatin Structure and Function, Institute for Quantitative Biosciences, The University of Tokyo, Tokyo 113-0032, Japan; [c]Cell Biology Center, Institute of Innovative Research, Tokyo Institute of Technology, Yokohama 226-8503, Japan; [d]Division of Transcriptomics, Medical Institute of Bioregulation, Kyushu University, Fukuoka 812-0054, Japan

Keywords: histone, chromatin, H2A, H2A.Z, H2A.X

Abstract

Histone proteins, including their variants, play indispensable roles in chromatin structure and function. The incorporation of specific histones is the key to epigenetic features and contributes to cell differentiation and development. To understand how each histone is targeted to and incorporated into a specific chromatin region, we introduced epitope-tagged histone complexes into permeabilized cells and allowed them to become incorporated into the chromatin. The newly incorporated histone complex is easily distinguished from the parental histones by the epitope-tag. We analyzed the correlation between the histone incorporation and the chromatin structure, using the H2A-H2B and H2A.Z-H2B complexes. The histone incorporation mainly occurred at less condensed chromatin (open), suggesting that the condensed chromatin (closed) is a barrier for histone incorporation. To overcome this barrier, H2A, but not H2A.Z, uses a replication-coupled deposition mechanism. This leads to the genome-wide distribution of H2A and the exclusion of H2A.Z from the closed chromatin. Moreover, H2A.Z-H2B is specifically incorporated into the chromatin around the transcription start sites. However, the H2A.Z mutant, in which the H2A.Z-specific region (M6) is swapped with the corresponding H2A residues, is incorporated into the closed chromatin in a replication-coupled manner. The mutant no longer functions as H2A.Z, in terms of the deposition. This may be the reason why the mutant does not compensate for the lethality of the H2A.Z knockout in flies. Our results show that histone incorporations are regulated by the chromatin structures, which may be crucial for maintaining the epigenetic chromatin states.

Introduction

Eukaryotic genomic DNA is packaged into chromatin, in which the basic structural unit is the nucleosome. The nucleosome is composed of around 150 base pairs of DNA and a histone octamer consisting of two copies of each core histone, H2A, H2B, H3, and H4 (1). Chromatin is not only the storage form of genomic DNA but also the regulator of DNA-templated processes, such as transcription, replication, repair, and chromosome segregation. To enable this, chromatin forms various structures, which can be reversibly altered. Historically, cytological studies first identified euchromatin and heterochromatin, which are transcriptionally active and inactive regions, respectively (2). Subsequent studies revealed that euchromatin coincides with nuclease hypersensitivity, indicating that it forms a more accessible structure (open chromatin) than heterochromatin (closed chromatin) (3-6). Although these chromatin structures are involved in the regulation of DNA template-mediated processes, little is known about how the open and closed chromatin configurations are formed and maintained.

Among the chromatin associated proteins, histones have a significant impact on the chromatin structure. In humans, the canonical histones, H2A, H2B, and H3.1, have non-allelic variants that show distinct expression and/or localization patterns (7, 8). Canonical H3.1 and H2A are expressed in S phase and show genome-wide localizations (8, 9). In contrast, the histone variants H3.3 and H2A.Z are expressed throughout the cell cycle and are concentrated at promoters in open chromatin (9-14). Another H2A variant, MacroH2A, localizes at transcriptionally suppressed chromatin, such as inactive X chromosomes (15). The localization of H2A.X, which functions in DNA repair, is genome-wide, along with the canonical H2A (16). Thus, in spite of the high sequence homology between the canonical and variant forms, each histone has specific functions. A previous study identified the essential 6 residues responsible

for the H2A.Z-specific functions, which are located in the αC helix called the M6 region (17). The H2A.Z swap mutant, in which M6 was replaced with the equivalent residues in H2A, failed to rescue the embryonic lethality of the H2A.Z null mutant in *Drosophila melanogaster*. Thus the importance of M6 was evident; however, the mechanism remained elusive.

The precise distribution of histones is crucial for chromatin organization and its epigenetic states. The ChIP-seq analysis is powerful and has visualized steady state histone localizations; however, it does not enable the analysis of the incorporation of each histone into open/closed chromatin or both (genome-wide). Histone deposition and exchange have been studied for more than 30 years (18-23). An *in vivo* histone deposition study must distinguish the pre-incorporated histones (parental histones) from the newly incorporated histones (new histones). To enable this, initial studies used radio-labeled histones and revealed that histone deposition occurred by both replication-coupled and replication-independent mechanisms (18, 19). More recently, fluorescent-based imaging methods, such as fluorescence recovery after photobleaching (FRAP) and SNAP/CLIP-tag technology, were developed to analyze the histone dynamics in living cells. FRAP is suitable for investigating the histone mobility in living cells (20, 22). The SNAP/CLIP-technology is effective for analyzing the histone deposition, as it can distinguish parental histones from new histones in cells with cell-permeable fluorophores that covalently bind to the tag (21, 23). Although these are powerful methods, they have resolution limitations, as they are based on imaging. The SNAP/CLIP-technology led to the establishment of the time-ChIP method, in which biotin labeled SNAP-histone is pulled down (24). The time-ChIP was developed to measure the stability of parental histones rather than analyzing histone incorporations (24, 25). To uncover the correlation between histone incorporation and open/closed chromatin structures, a new analysis of the histone incorporation at the DNA

sequence level is desired.

Permeabilized cells are useful to dissect apart molecular pathways in nuclear events (26, 27). In assays with such cells, the cellular membranes are permeabilized by a nonionic detergent treatment. In the permeabilized cells, chromatin and nuclear structures remain intact and react with exogenously added proteins (28-31). A previous study showed that an exogenously added GFP-tagged histone, which was prepared from cultured human cells, was incorporated into the chromatin of permeabilized cells in the presence of a cellular extract (31). Moreover, permeabilized cells are suitable for monitoring replication timing, by labeling the nascent DNA with exogenously introduced nucleotides (28, 31).

In the present study, we developed a new method, in which a reconstituted histone complex, instead of a fluorescent protein-tagged histone, was added to permeabilized cells. We named this the RhIP assay (Reconstituted histone complex Incorporation into chromatin of Permeabilized cell). Since the histone complexes are reconstituted *in vitro* using epitope-tagged recombinant histones, RhIP with sequencing allows us to analyze the incorporations at the DNA sequence level, without producing specific antibodies. Here we found that the chromatin structure regulates the histone incorporations, which may be necessary for maintaining the epigenetic state of chromatin.

Results

RhIP assay reproduces *in vivo* histone deposition. To understand how histones are incorporated within chromatin in cells, we developed the RhIP assay, in which an *in vitro* reconstituted histone complex, nucleotides, and a cellular extract are added to permeabilized cells (Fig. 1*A*). We first confirmed that the RhIP assay can recapitulate histone incorporations observed in cells. The H3.1-H4 incorporation into chromatin is coupled with replication, while the H3.3-H4 incorporation occurs throughout the cell cycle (10). We reconstituted H3-H4 complexes *in vitro*, using recombinant H3.1, H3.3, and H4 (Fig. 1*B*). H3.1 and H3.3 were fused to HA and FLAG at the C-termini, respectively. The permeabilized cells were then prepared by treating HeLa cells with a nonionic detergent, Triton X-100, and reconstituted H3-H4 complexes were added with the cellular extract and nucleotides. Cy5-dUTP was also added, in order to monitor DNA replication. After the reaction, exogenously added H3.1 and H3.3 were detected with antibodies against the HA and FLAG tags, respectively (Fig. 1*C* and *D*). As a result, the H3.1 was detected in Cy5 positive cells (S phase cells), while the H3.3 was detected irrespective of the Cy5 signal. These results indicate that the reconstituted H3.1-H4 and H3.3-H4 complexes were incorporated into the chromatin of permeabilized cells with the same dynamics observed in cells.

We next examined whether the cellular extract is essential or replaceable by histone chaperones, Nap1 or Asf1 (Fig. S1*A*). Nap1 and Asf1 bind to the H2A-H2B and H3-H4 complexes *in vivo*, respectively, and both promote nucleosome formation *in vitro* (32-34). Human Nap1 and Asf1 were purified as recombinant proteins (Fig. S1*B*). The H3.1-H4 complex was then added to the permeabilized cells in the absence of the cellular extract or in the presence of Nap1or Asf1, and the incorporation was analyzed by immunostaining (Fig. S1*C*).

Without the cellular extract or the histone chaperone, the exogenously added H3.1 was not detected in the permeabilized cells, indicating that no H3.1 incorporation had occurred. Nap1 promoted the promiscuous incorporation irrespective of DNA replication, and Asf1 facilitated H3.1 accumulation in the nucleoli. These data indicated that the functional deposition of the exogenously added histone complex requires the cellular extract, which may contain essential components. We conclude that the RhIP assay reproduces cellular histone deposition, and is suitable for analyzing histone incorporation *in vitro*.

H2A.Z incorporation into chromatin differs from that of H2A and H2A.X. Among the H2A family members, canonical H2A and the H2A.X variant show even and broad genome-wide distributions, but H2A.Z specifically localizes in open chromatin, including promoters and enhancers (8, 11). To test whether this difference reflects the manner of their deposition, we performed the RhIP assay (Fig. 2*A*). The H2A-H2B and H2A.Z-H2B complexes were reconstituted *in vitro* using recombinant proteins (Fig. 2*B*) and added to permeabilized cells, followed by immunostaining (Fig. 2*C*). The H2A and H2A.Z signals were both observed in the Cy5 negative and positive permeabilized cells, indicating that their incorporations occur irrespective of DNA replication. We also found that H2A forms foci in the S phase nuclei. We then merged the images of the H2A and Cy5 signals (Fig. 2*D*). The replication foci change as cells progress through S phase (35). In early S phase, the replication foci are present throughout the nucleoplasm, except for the nucleoli. The foci then accumulate in the nuclear periphery and around the nucleoli. In late S phase, the foci increase in size but decrease in number. We found that the H2A signals overlapped well with the replication foci throughout replication (Fig. 2*D*). The H2A.Z signals overlapped with the early replication foci to some extent (Fig. 2*E* image #4),

but they were clearly eliminated from the late replication foci (Fig. 2*E* images #5 and 6). In contrast to the difference between H2A and H2A.Z, the H2A and H2A.X signals overlapped well with each other, suggesting that their incorporation mechanism is the same (Fig. S2). These results indicate that H2A, H2A.X, and H2A.Z can be incorporated into chromatin in a replication-independent manner; however, during S phase, H2A and H2A.X are preferentially incorporated into the chromatin of ongoing replication sites, in contrast to the case for H2A.Z.

H2A is preferentially incorporated over H2A.Z into replicating chromatin. We further analyzed the incorporation of H2A and H2A.Z into replicating chromatin by RhIP, followed by a chromatin immunoprecipitation (RhIP-ChIP) assay (Fig. 3*A*). Reconstituted 3HA-H2A-H2B or 3HA-H2A.Z-H2B was added to permeabilized cells with the cellular extract and nucleotides, including Cy5-dUTP to label the nascent DNA (Fig. 3*A* and 3*B*). After the reaction, the chromatin was partially digested by micrococcal nuclease (MNase) and the nucleosomes containing 3HA-H2A or 3HA-H2A.Z were immunoprecipitated with an antibody against the HA tag. The precipitated DNA was then extracted and analyzed by gel electrophoresis. As shown in Fig. 3*C*, the amounts of precipitated DNA are nearly the same between the H2A and H2A.Z precipitants, judging from the SYBR Gold staining (Fig. 3*C*, upper); however, the amount of nascent DNA labeled with Cy5 is much more in the H2A precipitant than in the H2A.Z sample (Fig. 3*C*, lower). This result indicates that H2A is incorporated into replicating chromatin more efficiently than H2A.Z.

The replication timing in S phase strongly correlates with the chromatin configurations (36). In general, early and late replicating chromatin regions correspond to open and closed chromatin, respectively. We investigated whether the efficiencies of H2A and H2A.Z

incorporation into replicating chromatin change, according to the replication timing (Fig. S3). To analyze this, the cells were synchronized in early S phase by a double thymidine block, and then early and late S phase cells were collected at 0 and 5 hours post thymidine-release, respectively. The synchronized cells showed the typical early and late replication foci that were nascent DNA labeled with Cy5-dUTP (Fig. S3*A*). Using these cells, we performed RhIP-ChIP assays of H2A and H2A.Z. The results revealed that the incorporation efficiencies of both H2A and H2A.Z into replicating chromatin did not change, irrespective of the replication timing in S phase. This implies that the efficiencies of replication-coupled histone deposition are not different between open (early S-replicating) and closed (late S-replicating) chromatin (Fig. S3*B*).

Open and closed chromatin structures regulate histone deposition. The RhIP-ChIP assay showed that the replication-coupled deposition of H2A.Z was constant in the early and late S phases (Fig. 3*C* and S3). In contrast, the RhIP-immunostaining showed that more signals of H2A.Z incorporation were overlapped at the early replicating foci than the late replicating foci (Fig. 2*E*). This discrepancy may arise from the resolution of the RhIP-immunostaining imaging analysis. Some of the overlapping signals of H2A.Z and Cy5 in early S phase might represent the replication-independent H2A.Z deposition that occurred not exactly at, but close to the replication sites in open chromatin. To determine whether the efficiency of the replication-independent histone deposition depends on the open/closed chromatin configuration, we performed RhIP-ChIP-seq and analyzed how the H2A and H2A.Z incorporations occur in each type of chromatin (Fig. 4). First, we investigated replication-independent histone deposition using asynchronous permeabilized cells, in which the majority of the cells are out of S phase. We found that the RhIP-ChIP-seq profiles of H2A and H2A.Z showed specific peaks at

megabase resolution, which were not observed in the input samples (Fig. 4*A*). Furthermore, we noticed that these patterns are similar to the DNaseI-seq results, which mapped open chromatin regions (6), suggesting that H2A and H2A.Z are predominantly incorporated into open chromatin regions. To confirm this, we analyzed the efficiency of histone incorporations into open and closed chromatin using the chromHMM data (Core 15-state model), which classified chromatin into 15 states (37, 38) (Fig. 4*B*). The ChIP/input ratios of each chromatin region revealed that H2A and H2A.Z were efficiently incorporated into transcriptionally active open chromatin, while their incorporations into closed chromatin were inefficient. These results indicate that histone incorporation occurs mainly in the open chromatin regions in a replication-independent manner, and closed chromatin suppresses histone incorporation.

We then examined the efficiency of the histone incorporation into each chromatin region in S phase (Fig. 4*C*). We performed RhIP-ChIP-seq with synchronized cells in early or late S phase. The results revealed that the efficiency of H2A incorporation into open chromatin decreased in S phase progression, while in contrast, the incorporation into closed chromatin increased (Fig. 4*C*, compare magenta and green bars of H2A). Considering the fact that the open and closed chromatin are respectively replicated in early and late S phase, the changes in the incorporation efficiency correlated with the changes in replicating chromatin. Together with the results shown in Fig. 4*B*, we concluded that the H2A-H2B incorporation into open chromatin occurs in both replication-independent (Fig. 4*B*) and -coupled (Fig. 4*C*) manners, but the H2A-H2B incorporation into closed chromatin occurs in a replication-coupled manner in late S phase (Fig. 4*C*). Therefore, replication is required for the incorporation of H2A into closed chromatin. Consistent with this, the correlation coefficients of the H2A RhIP-ChIP-seq data in early and late S phase showed a weak relationship (Fig. 4*D*). On the other hand, the

H2A.Z incorporation efficiencies were almost the same in the early and late S phases (Fig. 4*C*, compare magenta and green bars of H2A.Z). The correlation coefficients revealed the strong relationship between the early S and late S samples (Fig. 4*D*). This indicates that, in principle, H2A.Z-H2B incorporation into chromatin is not coupled with replication, which leads to H2A.Z elimination from closed chromatin.

The M6 domain of H2A.Z is important for H2A.Z-specific deposition. Our RhIP-ChIP-seq analysis demonstrated that H2A.Z was incorporated efficiently into open chromatin, especially at transcription start sites (TSS) (Fig. 4*B*). The comparison of the H2A.Z incorporation peaks in RhIP-ChIP-seq with the steady state ChIP-seq data (39) highlighted their similarities (Fig. 5*A* and *B*). This indicated that H2A.Z deposition mainly determines its specific localization. We then tried to identify the residues responsible for the H2A.Z-specific deposition by a mutant analysis. A previous study showed that swapping the M6 region of H2A.Z with the corresponding H2A residues could not rescue the embryonic lethality of the H2A.Z null mutation in *Drosophila melanogaster* (17), suggesting that the region specifies the H2A.Z identity. The H2A.Z-specific residues in the M6 region are exposed on the surface of the H2A.Z-H2B dimer, but are buried inside the nucleosome, except for Gly 92 (40, 41) (Fig. 5*C*, cyan). This suggests that the M6 region is important for the H2A.Z deposition, since other proteins can recognize it before the deposition, but not after nucleosome formation. To test this idea, we constructed the swapped mutant (H2A.Z_M6) and performed the RhIP assay (Fig. 5*D*-*F*). Surprisingly, H2A.Z_M6-H2B formed foci in late replicating chromatin (Fig. 5*E*) and its incorporation pattern was more similar to that of H2A-H2B, rather than H2A.Z-H2B (Fig. 5*F*). This indicated that the mutant is no longer H2A.Z, in terms of deposition. Thus, the M6 region

of H2A.Z is responsible for the H2A.Z-specific deposition. This also means that the corresponding region (amino acids 89-100) of H2A is responsible for the replication-coupled H2A deposition.

Discussion

In the present study, we revealed the correlation between histone incorporation and chromatin structure, using the RhIP assay. We analyzed the incorporation of the H2A family members, H2A, H2A.X, and H2A.Z (Figs. 2-5, S2 and S3). We found that the incorporations of H2A-H2B and H2A.X-H2B into transcriptionally active open chromatin can occur in both replication-coupled and independent manners, whereas their incorporation into transcriptionally inactive closed chromatin occurs only in a replication-coupled manner in late S phase (Figs. 4 and 6). This indicated that there is little chance for histone exchange in closed chromatin. The genome-wide localization of H2A and H2A.X is achieved by a combination of deposition into open chromatin and replication-coupled deposition into closed chromatin (Fig. 6). In contrast, H2A.Z exhibited a much lower frequency of replication-coupled deposition, as compared to H2A (Fig. 3*C* and S3*B*). Together with the fact that the amount of H2A.Z is much lower than that of than H2A in S phase in cells (9), we concluded that little to no H2A.Z is incorporated into closed chromatin (Fig. 6). This is consistent with previous observations that H2A.Z and DNA methylation localization are mutually exclusive (42, 43), and that H2A.Z predominantly exists at promoters and enhancers (8, 11). It had been unclear how H2A.Z is enriched at specific regions of open chromatin. Our study suggested that H2A.Z elimination from transcriptionally inactive chromatin is due to the low frequencies of histone exchange and the replication-coupled H2A.Z incorporation, which may partially explain the H2A.Z distribution pattern (Fig. 6).

Moreover, H2A.Z was specifically incorporated into chromatin around the TSS in the RhIP assay, which is exactly the same as the steady state localization of H2A.Z revealed by ChIP-seq (39) (Fig. 5*A*). There may be the mechanism for H2A.Z targeting to the TSS.

Another H2A variant, MacroH2A, localizes in closed chromatin. A recent study showed that the *de novo* incorporation of MacroH2A is genome-wide. It is then removed from transcribed chromatin in a transcription-associated mechanism, leading to the specific localization at repressed chromatin (44). Our data may be able to explain why this two-step mechanism is needed for MacroH2A localization in closed chromatin. We showed that H2A is incorporated into closed chromatin in a replication-coupled manner. If MacroH2A also uses the replication-coupled deposition mechanism, then it is inevitably incorporated into closed and open chromatin, first resulting in the genome-wide distribution. MacroH2A must then be removed from the active chromatin for its specific closed chromatin localization.

We found that histone incorporations are regulated by the chromatin structure, which may be important for maintaining the closed chromatin configuration. Histones reportedly form a pre-deposition complex, which includes many transcription-related factors, before their incorporation into chromatin *in vivo* (45-48). For instance, the H2A-H2B pre-deposition complex contains Spt16 and SSRP1, which form a heterodimer complex called FACT that functions in transcription facilitation, and the pre-deposition H2A.Z-H2B complex also includes a chromatin remodeling factor (SRCAP), a histone acetyltransferase (Tip60), and acetyl-lysine binding proteins (GAS41, Brd8). If histone exchange usually occurs in closed chromatin, then these transcription-related factors might accumulate in the closed chromatin and alter the epigenetic chromatin states. Therefore, the deficiency of replication-independent histone exchange in closed chromatin may be important for maintaining a transcriptionally inactive

state.

In spite of the high sequence homology between H2A and H2A.Z, their localizations are different. By using the swapping mutant, we analyzed the residues responsible for the specific depositions of H2A and H2A.Z (Fig. 5). We identified residues 88-100 of H2A as being responsible for its replication-coupled deposition. It is unknown how this region contributes to the incorporation into replicating chromatin, but a factor that binds this region and allows H2A to assemble at a replicating site may exist. The major H2A-specific chaperones, Spt16 and Nap1, which are components of the H2A pre-deposition complex, do not bind to this region (49, 50). Thus, the binding protein for the residues is likely to be a chromatin protein involved in replication, rather than a component of the H2A pre-deposition complex. This region is a counterpart of the H2A.Z M6 region (17). It was unclear why the H2A.Z_M6 swapping mutant did not compensate for the embryonic lethality of the H2A.Z knockout in *Drosophila melanogaster* (17). Our data indicated that the H2A.Z_M6 mutant is incorporated into closed chromatin in a replication-coupled manner, suggesting that the genome-wide localization of the H2A.Z mutant may result in aberrant gene expression, leading to impaired embryonic development.

Taken together, our novel method elucidated the mechanism of histone incorporation at the DNA sequence level, and revealed that the chromatin structure is the first determinant of histone localization.

Materials and Methods

Cell culture and thymidine block

HeLa cells were cultured in DMEM medium supplemented with 10% fetal bovine

serum, at 37°C in 5% CO_2. For cell synchronization, HeLa cells were cultured with 2 mM thymidine for 19 hours. The medium was then changed to remove the thymidine. After 9 hours of culture without thymidine, the HeLa cells were cultured with 2 mM thymidine again for 15 hours, to synchronize the HeLa cells in S phase.

Reconstitution of histone complex

The human H3.1 and H3.3 genes were inserted in the pET21a vector (Novagen), as C-terminal epitope-tag-His_6 fused genes. The human H2A, H2A.X, H2A.Z, and H2A.Z_M6 genes were inserted in the pET15b vector (Novagen) as N-terminal His6-epitope-tag fused genes. All of the genes were overexpressed in the BL21(DE3) *E. coli* strain, by adding 0.5 mM isopropyl-β-D-thiogalactopyranoside. Each histone was then purified as described previously, using Ni-NTA affinity chromatography (22). The epitope tag-fused histones were freeze-dried without removing the His_6 tags. Human H2B and H4 were overexpressed and purified after removing the Hi_6 tags, as described previously (22). Freeze-dried H3.1 or H3.3 was mixed with H4 and H2A, H2A.X, H2A.Z, and H2A.Z_M6, mixed with H2B in 20 mM Tris-HCl buffer (pH 7.5), containing 7 M guanidine hydrochloride and 20 mM 2-mercaptoethanol, and incubated on ice. After 1 hour, the samples were dialyzed against the reconstitution buffer (10 mM Tris-HCl buffer (pH 7.5) and 2 mM 2-mercaptoethanol) containing 2 M NaCl, overnight at 4°C. The NaCl concentration was then decreased by three steps of dialysis against the reconstitution buffer containing 1 M NaCl for 4 hours, 0.5 M NaCl for 4 hours, and 0.1 M NaCl overnight. After the dialyses, the precipitants were removed by centrifugation and the supernatants were analyzed by Superdex 200 gel filtration chromatography (GE Healthcare).

RhIP assay

Cell permeabilization was performed as described previously, with minor modifications (31). HeLa cells were chilled on ice and rinsed twice with ice-cold PBF (100 mM CH_3COOK, 10 mM Na_2HPO_4, 30 mM KCl, 1 mM dithiothreitol, 1 mM $MgCl_2$, 1 mM ATP, and 5% Ficoll). Afterwards, PBF containing 0.2% Triton X-100 was added to the cells. After a 5 min incubation on ice, the permeabilized cells were rinsed twice with ice-cold PBF. The preparation of the cellular extract was described previously, as a cytosolic extract (51). The histone incorporation assay was performed as described previously, with modifications (31). A reaction mixture containing 100 nM histone complex, 60% cellular extract, 2.5% Ficoll, 100 mM CH_3COOK, 10 mM Na_2HPO_4, 30 mM KCl, 1 mM dithiothreitol, 1 mM $MgCl_2$, 100 µM each of dNTPs, and NTPs (Roche) with or without 250 nM Cy5-dUTP (Enzo Life Sciences), was added to the permeabilized cells. After 60 min at 30°C, the cells were washed in PBS containing 0.05% Tween 20 (PBST) twice, for 5 min at room temperature.

RhIP-immunostaining

After the RhIP assay, the cells were fixed with 4% PFA (Electron Microscopy Sciences) in PBS for 20 min at room temperature, and rinsed three times with PBS. After fixation, the cells were treated with 1% BSA in PBST for 1 hour at room temperature, and then with the primary antibodies in the same buffer. After 2 hours at room temperature, the cells were washed in PBST three times for 10 min, treated with the secondary antibodies for 1 hour at room temperature, and washed in PBST three times for 10 min. DNA was stained with Hoechst 33342. The samples were mounted with ProLong Gold (Life Technologies). All images were acquired by using the Deltavision set-up (GE Healthcare) with an inverted Olympus IX71

microscope, equipped with a CoolSNAP ES2 CCD camera (Photometrics) and a 60×, 1.42 Plan Apo N Olympus oil-immersion objective. Image files were converted to the TIFF format using the ImageJ software (52) and imported into Illustrator (Adobe) for assembly. The co-localization analysis was performed using ImageJ Colocalization_Finder plugin.

RhIP-ChIP

After the RhIP assay, the chromatin was digested with micrococcal nuclease (MNase) as described previously (53). The reaction was terminated by adding 10 mM EDTA, and the solubilized chromatin fragments were separated from the pellets by centrifugation at 16,000g for 5 min at 4°C. The samples were then mixed with 50 µl of anti-HA-tag mAb-Magnetic Beads (MBL International) in 15 mM Tris-HCl, pH 7.5, 300 mM NaCl, and 0.1% NP-40. After an overnight incubation at 4°C with gentle mixing on a wheel, the beads were washed twice with 1 ml of wash buffer (10 mM Tris-HCl, pH 7.5, 2 mM EDTA, 500 mM NaCl, and 0.1% Triton X-100). The DNA was then eluted with a Proteinase K solution (20 mM Tris-HCl, pH 8.0, 20 mM EDTA, 0.5% sodium dodecyl sulfate (SDS), and 0.5 mg/ml Proteinase K) and extracted with phenol-chloroform. The DNA was precipitated with ethanol and resuspended in 10 mM Tris-HCl, pH 8.0, and 1 mM EDTA. The resulting DNAs were separated by electrophoresis on a 2% agarose gel (7.4 V/cm, 35 min) or a 1.5 % agarose gel (7.1 V/cm, 60 min) in 1×TAE, and stained with SYBR Gold (Thermo Fisher). Images of the DNA stained with SYBR Gold and the nascent DNA labeled with Cy5 were obtained with an Amersham Typhoon scanner (GE Healthcare).

RhIP-ChIP-seq

After the RhIP assay, the permeabilized cells were treated with 3% formaldehyde in PBS for 5 min at room temperature. The fixed chromatin of the permeabilized cells was digested with MNase in ChIP buffer (10 mM Tris-HCl, pH 8.0, 200 mM KCl, 1 mM $CaCl_2$, 0.5% NP-40). The supernatant was incubated with 50 µl of anti-HA-tag mAb-Magnetic Beads, and gently mixed by rotation at 4°C overnight. The beads were then washed three times with ChIP buffer containing 500 mM KCl and TE. After the beads were washed, they were resuspended in 100 µl of ChIP elution buffer (50 mM Tris-HCl, pH 8.0, 10 mM EDTA, and 1% SDS) containing 25 mM NaCl, and incubated overnight at 65°C to reverse the cross-links. The DNA was then eluted with 0.4 mg/ml Proteinase K. The eluted DNA samples were further purified with a NucleoSpin Gel and PCR clean-up kit (MACHEREY-NAGEL). The DNA libraries were prepared using a SMARTer ThruPLEX Tag-seq Kit (Takara Bio), and the samples were sequenced on an Illumina HiSeq1500 system.

ChIP-Seq data analysis

The in-read unique-molecular-identifiers (tags) were extracted using UMI-tools (54) with the command: umi_tools extract --extract-method=regex --bc-pattern='(?P<umi_1>.{6})(?P<discard_1>.{0,3}GTAGCTCA){s<=2}'. The extracted reads were mapped to the human genome (GRCh38) using hisat2 (version 2.1.0) (55). The PCR-duplicates were removed using umi_tools dedup. The read counts on 15 chromatin states were calculated using BED-Tools (56). The definition of the ChromHMM track was obtained from the consolidated data set of the Roadmap Epigenomics project (E117_15_coreMarks_hg38lift_mnemonics.bed) (38). The overall concentrations of the ChIP signals (log2 ratio) were calculated as the ratio of the proportion of reads in each chromatin

state between the ChIP and input DNA data; i.e., $\log_2$(ChIP/Input) after normalization of the total reads. The signal tracks (bigwig files) were created by 1 bp intervals on the genome, and then the counts were normalized as CPM (Reads Per Million reads), using deepTools (57). ChIP-seq signals were visualized with the Integrative Genomics Viewer, IGV (58). The Pearson correlation coefficients were calculated throughout 1,000 bp intervals with the multiBigwigSummary program of deepTools, and plotted with the plotCorrelation program (57). The computeMatrix program of deepTools was utilized to analyze the percentages of peak localizations around the TSS.

Purification of Nap1 and Asf1

Human Nap1 was purified as described previously (34). The human Asf1 gene was inserted in the pET15b vector (Novagen), in which the thrombin proteinase recognition sequence was replaced by the PreScission proteinase recognition sequence. The *Escherichia coli* strain BL21-CodonPlus (DE3)-RIL (Agilent Technologies) was freshly transformed with the vector, and cultured at 30°C. After the cell density reached an A_{600} = 0.8, 1 mM isopropyl-β-D-thiogalactopyranoside was added and the culture was continued at 18°C for 12 h to induce His_6-tagged Asf1 expression. The cells were collected and resuspended in 20 mM Tris-HCl, pH 7.5, containing 500 mM KCl, 10% glycerol, 0.1% NP-40, 1 mM phenylmethylsulfonyl fluoride (PMSF), and 2 mM 2-mercaptoethanol. After disruption by sonication, the cell debris was removed by centrifugation (27,216 ×g; 20 min), and the lysate was mixed gently with 4 ml (50% slurry) of nickel-nitrilotriacetic acid (Ni-NTA)-agarose resin (Qiagen) at 4°C for 1 h. The Ni-NTA beads were washed with 200 ml of 20 mM Tris-HCl, pH 7.5, containing 500 mM NaCl, 10% glycerol, 10 mM imidazole, and 2 mM 2-mercaptoethanol. The His_6-tagged Asf1 was

eluted by a 100-ml linear gradient of imidazole from 10 to 500 mM in 50 mM Tris-HCl buffer (pH 7.5), containing 500 mM NaCl, 10% glycerol, and 2 mM 2-mercaptoethanol. PreScission proteinase (8 units/mg of protein, GE Healthcare) was added to remove the His_6 tag from the Asf1. The sample was dialyzed against 20 mM Tris-HCl, pH 7.5, containing 100 mM NaCl, 1 mM EDTA, 10% glycerol, and 2 mM 2-mercaptoethanol. The Asf1 was further purified using a Mono Q (GE Healthcare) column, by elution with a 25-ml linear gradient of 100–600 mM NaCl in 20 mM Tris-HCl, pH 7.5, containing 1 mM EDTA, 10% glycerol, and 2 mM 2-mercaptoethanol. The eluted Asf1 was further purified using a Superdex 75 (GE Healthcare) column, eluted with 1.2 column volumes of the same buffer containing 100 mM NaCl. The Asf1 was again purified by Mono Q chromatography and concentrated. Finally, the Asf1 was dialyzed against 20 mM Tris-HCl (pH 7.5), containing 150 mM NaCl, 1 mM dithiothreitol, 0.5 mM EDTA, 0.1 mM PMSF, and 10% glycerol.

Antibodies

For immunostaining, anti-HA (mouse, 1/1000, Santa Cruz sc-7392), anti-DDDDK (FLAG) (rabbit, 1/500, MBL, PM020), or anti-V5 (chicken, 1/1000, Abcam, ab9113) was used as the primary antibody. Goat Alexa Fluor 488 or 546-conjugated anti-mouse IgG (Life Technology), or goat DyLight 488 or 550-conjugated anti-rabbit IgG or chicken IgY (Thermo Fisher) was used as the secondary antibody.

Data Availability

The deep sequencing data in this study are publicly available at the accession number GEO: GSE130947.

Acknowledgments

This work was supported by JSPS KAKENHI Grant Numbers 17H05013, 16K14785 (to H.T.), 18H05531, 18K19310 (to N.S.), 18H04904, 19H04970, 19H03158 (to K.M.), 18K19432, 19H05425, 19H03211 (to A.H.), 17K19356, 17H03608, 18H05527, 18H04802, 19H05244 (to Y.O.), and JST CREST grants (JPMJCR16G1 to Y.O. H.Kurumizaka and H.Kimura), JP18H05534 and JP17H01408 (to H.Kurumizaka), 17H01417, and 18H05527 (to H.Kimura). We thank Dr. Crawford at Duke University for the DNaseI-seq data (GEO:GSM816643), Dr. Bernstein at the Broad Institute for the H2A.Z ChIP-seq data (GEO:GSM1003483), and the ENCODE Consortium. H.T. is supported by The Nakajima Foundation. N.S. is supported by the Naito Foundation, the Takeda Science Foundation, and the Sharyo Foundation.

References

1. Luger K, Mäder AW, Richmond RK, Sargent DF, Richmond TJ (1997) Crystal structure of the nucleosome core particle at 2.8 Å resolution. *Nature* 389(6648):251–260.

2. Passarge E (1979) Emil Heitz and the concept of heterochromatin: longitudinal chromosome differentiation was recognized fifty years ago. *Am J Hum Genet* 31(2):106–115.

3. Weintraub H, Groudine M (1976) Chromosomal subunits in active genes have an altered conformation. *Science* 193(4256):848–856.

4. Garel A, Axel R (1976) Selective digestion of transcriptionally active ovalbumin genes from oviduct nuclei. *Proc Natl Acad Sci USA* 73(11):3966–3970.

5. Spiker S, Murray MG, Thompson WF (1983) DNase I sensitivity of transcriptionally active genes in intact nuclei and isolated chromatin of plants. *Proc Natl Acad Sci USA* 80(3):815–819.

6. Tsompana M, Buck MJ (2014) Chromatin accessibility: a window into the genome. *Epigenetics Chromatin* 7(1):33.

7. Maehara K, et al. (2015) Tissue-specific expression of histone H3 variants diversified after species separation. *Epigenetics Chromatin* 8(1):35.

8. Buschbeck M, Hake SB (2017) Variants of core histones and their roles in cell fate decisions, development and cancer. *Nat Rev Mol Cell Biol* 18(5):299–314.

9. Wu RS, Tsai S, Bonner WM (1982) Patterns of histone variant synthesis can distinguish G0 from G1 cells. *Cell* 31(2 Pt 1):367–374.

10. Ahmad K, Henikoff S (2002) The histone variant H3.3 marks active chromatin by replication-independent nucleosome assembly. *Mol Cell* 9(6):1191–1200.

11. Raisner RM, et al. (2005) Histone variant H2A.Z marks the 5' ends of both active and inactive genes in euchromatin. *Cell* 123(2):233–248.

12. Jin C, Felsenfeld G (2007) Nucleosome stability mediated by histone variants H3.3 and H2A.Z. *Genes Dev* 21(12):1519–1529.

13. Jin C, et al. (2009) H3.3/H2A.Z double variant-containing nucleosomes mark "nucleosome-free regions" of active promoters and other regulatory regions. *Nat Genet* 41(8):941–945.

14. Goldberg AD, et al. (2010) Distinct factors control histone variant H3.3 localization at specific genomic regions. *Cell* 140(5):678–691.

15. Costanzi C, Stein P, Worrad DM, Schultz RM, Pehrson JR (2000) Histone macroH2A1 is concentrated in the inactive X chromosome of female preimplantation mouse embryos. *Development* 127(11):2283–2289.

16. Yukawa M, et al. (2014) Genome-wide analysis of the chromatin composition of histone H2A and H3 variants in mouse embryonic stem cells. *PLoS ONE* 9(3):e92689.

17. Clarkson MJ, Wells JR, Gibson F, Saint R, Tremethick DJ (1999) Regions of variant histone His2AvD required for *Drosophila* development. *Nature* 399(6737):694–697.

18. Louters L, Chalkley R (1985) Histones H1, H2A, and H2B in Vivo. *Biochemistry* 24(13):3080–3085.

19. Jackson V (1990) In Vivo Studies on the Dynamics of Histone-DNA Interaction: Evidence for Nucleosome Dissolution during Replication and Transcription and a Low Level of Dissolution Independent of Both. *Biochemistry* 29(3):719–731.

20. Kimura H, Cook PR (2001) Kinetics of core histones in living human cells: little exchange of H3 and H4 and some rapid exchange of H2B. *J Cell Biol* 153(7):1341–1353.

21. Jansen LET, Black BE, Foltz DR, Cleveland DW (2007) Propagation of centromeric chromatin requires exit from mitosis. *J Cell Biol* 176(6):795–805.

22. Tachiwana H, et al. (2010) Structural basis of instability of the nucleosome containing a testis-specific histone variant, human H3T. *Proc Nat Aca Sci USA* 107(23):10454–10459.

23. Ray-Gallet D, et al. (2011) Dynamics of histone H3 deposition in vivo reveal a nucleosome gap-filling mechanism for H3.3 to maintain chromatin integrity. *Mol Cell* 44(6):928–941.

24. Deaton AM, et al. (2016) Enhancer regions show high histone H3.3 turnover that changes during differentiation. *Elife* 5:e1002358.

25. Siwek W, Gómez-Rodríguez M, Sobral D, Corrêa IR, Jansen LET (2018) time-ChIP: A Method to Determine Long-Term Locus-Specific Nucleosome Inheritance. *Methods Mol Biol* 1832:131–158.

26. Adam SA, Marr RS, Gerace L (1990) Nuclear protein import in permeabilized mammalian cells requires soluble cytoplasmic factors. *J Cell Biol* 111(3):807–816.

27. Okuno Y, Imamoto N, Yoneda Y (1993) 70-kDa heat-shock cognate protein colocalizes with karyophilic proteins into the nucleus during their transport in vitro. *Exp Cell Res* 206(1):134–142.

28. Misteli T, Spector DL (1996) Serine/threonine phosphatase 1 modulates the subnuclear distribution of pre-mRNA splicing factors. *Mol Biol Cell* 7(10):1559–1572.

29. Maison C, et al. (2002) Higher-order structure in pericentric heterochromatin involves a distinct pattern of histone modification and an RNA component. *Nat Genet* 30(3):329–334.

30. Saitoh N, et al. (2006) In situ SUMOylation analysis reveals a modulatory role of RanBP2 in the nuclear rim and PML bodies. *Exp Cell Res* 312(8):1418–1430.

31. Kimura H, et al. (2006) A Novel Histone Exchange Factor, Protein Phosphatase 2Cγ, Mediates the Exchange and Dephosphorylation of H2A-H2B. *J Cell Biol* 175(3):389–400.

32. Ishimi Y, et al. (1984) Purification and initial characterization of a protein which facilitates assembly of nucleosome-like structure from mammalian cells. *Eur J Biochem* 142(3):431–439.

33. Munakata T, Adachi N, Yokoyama N, Kuzuhara T, Horikoshi M (2000) A human homologue of yeast anti-silencing factor has histone chaperone activity. *Genes Cells* 5(3):221–233.

34. Tachiwana H, Osakabe A, Kimura H, Kurumizaka H (2008) Nucleosome formation with the testis-specific histone H3 variant, H3t, by human nucleosome assembly proteins *in vitro*. *Nucleic Acids Res* 36(7):2208–2218.

35. Leonhardt H, et al. (2000) Dynamics of DNA replication factories in living cells. *J Cell*

Biol 149(2):271–280.

36. Rivera-Mulia JC, Gilbert DM (2016) Replication timing and transcriptional control: beyond cause and effect — part III. *Current Opinion in Cell Biology* 40:168–178.

37. Ernst J, Kellis M (2012) ChromHMM: automating chromatin-state discovery and characterization. *Nat Methods* 9(3):215–216.

38. Roadmap Epigenomics Consortium, et al. (2015) Integrative analysis of 111 reference human epigenomes. *Nature* 518(7539):317–330.

39. ENCODE Project Consortium (2012) An integrated encyclopedia of DNA elements in the human genome. *Nature* 489(7414):57–74.

40. Suto RK, Clarkson MJ, Tremethick DJ, Luger K (2000) Crystal structure of a nucleosome core particle containing the variant histone H2A.Z. *Nat Struct Biol* 7(12):1121–1124.

41. Horikoshi N, et al. (2013) Structural polymorphism in the L1 loop regions of human H2A.Z.1 and H2A.Z.2. *Acta Crystallogr D Biol Crystallogr* 69(Pt 12):2431–2439.

42. Zilberman D, Coleman-Derr D, Ballinger T, Henikoff S (2008) Histone H2A.Z and DNA methylation are mutually antagonistic chromatin marks. *Nature* 456(7218):125–129.

43. Nothjunge S, et al. (2017) DNA methylation signatures follow preformed chromatin compartments in cardiac myocytes. *Nat Commun* 8(1):1667.

44. Sun Z, et al. (2018) Transcription-associated histone pruning demarcates macroH2A chromatin domains. *Nat Struct Mol Biol* 25(10):958–970.

45. Tagami H, Ray-Gallet D, Almouzni G, Nakatani Y (2004) Histone H3.1 and H3.3 complexes mediate nucleosome assembly pathways dependent or independent of DNA synthesis. *Cell* 116(1):51–61.

46. Dunleavy EM, et al. (2009) HJURP Is a Cell-Cycle-Dependent Maintenance and Deposition Factor of CENP-A at Centromeres. *Cell* 137(3):485–497.

47. Mao Z, et al. (2014) Anp32e, a higher eukaryotic histone chaperone directs preferential

recognition for H2A.Z. *Cell Res* 24(4):389–399.

48. Obri A, et al. (2014) ANP32E is a histone chaperone that removes H2A.Z from chromatin. *Nature* 505(7485):648–653.

49. Kemble DJ, McCullough LL, Whitby FG, Formosa T, Hill CP (2015) FACT Disrupts Nucleosome Structure by Binding H2A-H2B with Conserved Peptide Motifs. *Mol Cell* 60(2):294–306.

50. Aguilar-Gurrieri C, et al. (2016) Structural evidence for Nap1-dependent H2A-H2B deposition and nucleosome assembly. *EMBO J* 35(13):1465–1482.

51. Martini E, Roche DM, Marheineke K, Verreault A, Almouzni G (1998) Recruitment of phosphorylated chromatin assembly factor 1 to chromatin after UV irradiation of human cells. *J Cell Biol* 143(3):563–575.

52. Schneider CA, Rasband WS, Eliceiri KW (2012) NIH Image to ImageJ: 25 years of image analysis. *Nat Methods* 9(7):671–675.

53. Tachiwana H, et al. (2015) HJURP involvement in de novo CenH3(CENP-A) and CENP-C recruitment. *Cell Rep* 11(1):22–32.

54. Smith T, Heger A, Sudbery I (2017) UMI-tools: modeling sequencing errors in Unique Molecular Identifiers to improve quantification accuracy. *Genome Res* 27(3):491–499.

55. Kim D, Langmead B, Salzberg SL (2015) HISAT: a fast spliced aligner with low memory requirements. *Nat Methods* 12(4):357–360.

56. Quinlan AR, Hall IM (2010) BEDTools: a flexible suite of utilities for comparing genomic features. *Bioinformatics* 26(6):841–842.

57. Ramírez F, Dündar F, Diehl S, Grüning BA, Manke T (2014) deepTools: a flexible platform for exploring deep-sequencing data. *Nucleic Acids Res* 42(Web Server issue):W187–91.

58. Robinson JT, et al. (2011) Integrative genomics viewer. *Nat Biotechnol* 29(1):24–26.

Figure Legends

Fig. 1. RhIP (Reconstituted histone complex Incorporation into chromatin of Permeabilized cells) assay, using H3.1-H4 and H3.3-H4 complexes. (*A*) Schematic representation of the RhIP assay, using reconstituted H3.1-H4 and H3.3-H4 complexes. Permeabilized cells were prepared from HeLa cells treated with non-ionic detergent, to perforate the cellular membranes. The *in vitro* reconstituted H3-H4 complexes were then added to the cells with the cellular extract and nucleotides. Cy5-dUTP was added to label the nascent DNA, so replication could be monitored. (*B*) Reconstituted H3.1-H4 and H3.3-H4 complexes were analyzed by SDS-16% PAGE with Coomassie Brilliant Blue staining. 3HA and 3FLAG were fused to the C-termini of H3.1 and H3.3, respectively. Lane 1 indicates the molecular mass markers, and lanes 2 and 3 indicate the H3.1-H4 and H3.3-H4 complexes, respectively. (*C*) RhIP-immunostaining of H3.1 and H3.3. Exogenously added H3-H4 complexes were stained with an anti-HA or FLAG antibody. Cells in S phase were monitored with Cy5-dUTP, which was incorporated into the nascent DNA. Bar indicates 10 μm. (*D*) Quantification of Fig. 1C. The mean fluorescence intensities (MFI) of H3.1-3HA (left) and H3.3-3FLAG (right) were measured. Nuclei were divided into S phase (Cy5 positive) and out of S phase (Cy5 negative) (n>150).

Fig. 2. Analysis of histone H2A and H2A.Z incorporations with the RhIP assay. (*A*) Schematic representation of the RhIP assay, using the reconstituted H2A-H2B and H2A.Z-H2B complexes. (*B*) The reconstituted H2A-H2B and H2A.Z-H2B complexes were analyzed by SDS-16% PAGE with Coomassie Brilliant Blue staining. 3HA and V5 were fused to the N-termini of H2A and H2A.Z, respectively. Lane 1 indicates the molecular mass markers, and lanes 2 and 3 indicate the H2A-H2B and H2A.Z-H2B complexes, respectively. (*C*) RhIP-immunostaining of

H2A and H2A.Z. Top: Exogenously added H2A-H2B complexes were stained with either an anti-HA or V5 antibody. Cells in S phase were monitored with Cy5-dUTP. (*D* and *E*) Top: merged images of Cy5-dUTP (green) and H2A (*D*), or H2A.Z (*E*) (red). The boxed areas in the left panels are enlarged and shown on the right. Bar indicates 10 μm. Bottom: pixel-by-pixel co-localization analyses. Scatter plots of Cy5-dUTP intensities versus H2A (*D*) or H2A.Z (*E*) intensities were shown. r indicates the Pearson correlation coefficient.

Fig. 3. Analysis of histone H2A and H2A.Z incorporations with the RhIP-ChIP assay. (*A*) Schematic representation of the RhIP-ChIP assay, using the reconstituted H2A-H2B and H2A.Z-H2B complexes. The reconstituted H2A-H2B or H2A.Z-H2B complex was added to permeabilized cells with the cellular extract and nucleotides. Cy5-dUTP was added to label the nascent DNA. The chromatin was partially digested with micrococcal nuclease (MNase). Chromatin immunoprecipitation was performed with anti-HA magnetic beads. The precipitated DNA was extracted and analyzed by agarose gel electrophoresis. (*B*) Reconstituted H2A-H2B and H2A.Z-H2B complexes were analyzed by SDS-16% PAGE with Coomassie Brilliant Blue staining. 3HA was fused to the N-termini of H2A and HA.Z. Lane 1 indicates the molecular mass markers, and lanes 2 and 3 indicate the H2A-H2B and H2A.Z-H2B complexes, respectively. (*C*) The immunoprecipitated DNA was analyzed by 2% agarose electrophoresis. Upper and lower images were obtained from the same gel. The DNA was visualized with SYBR Gold (upper), and the nascent DNA was visualized by detecting the Cy5 signals (lower). Lane 1 indicates the 100 bp DNA ladder. Lanes 2-4 and 5-7 indicate input samples and immunoprecipitated samples, respectively. Each lane indicates a negative control without adding the reconstituted histone complex (lanes 2 and 5), the samples with 3HA-H2A-H2B

(lanes 3 and 6), and the samples with 3HA-H2A.Z-H2B (lanes 4 and 7).

Fig. 4. RhIP-ChIP-seq analysis of H2A and H2A.Z. (*A*) RhIP-ChIP-seq and DNaseI-seq profiles using asynchronous cells were visualized with the Integrative Genomics Viewer. From top to bottom, profiles of H2A (RhIP-ChIP), H2A.Z (RhIP-ChIP), DNaseI-seq (GEO:GSM816643), input (RhIP-ChIP, H2A), and input (RhIP-ChIP, H2A.Z) are indicated. (*B*) Enrichment of incorporated H2A or H2A.Z in each chromatin region, previously annotated by the Roadmap Epigenomics project. Each abbreviation means TssA: active TSS, TssAFlnk: flanking active TSS, TxFlnk: transcribed state at the 5' and 3' ends of genes showing both the promoter and enhancer signatures, Tx: strong transcription, TxWk: weak transcription, EnhG: genic enhancers, Enh: enhancers, TssBiv: bivalent/poised TSS, BivFlnk: flanking bivalent TSS/enhancers, EnhBiv: bivalent enhancers, ZNF/Rpts: ZNF genes & repeats, ReprPC: repressed PolyComb, ReprPCWk: weak repressed PolyComb, Het: heterochromatin, and Quies: quiescent/low (37, 38). Two biological replicates of H2A and H2A.Z are shown. (*C*) RhIP-ChIP-seq using synchronized cells in early or late S phase. Bar graphs indicate the enrichment of the incorporated H2A or H2A.Z in early or late S phase. Two biological replicates of H2A and H2A.Z are shown. (*D*) The Pearson correlation coefficients between early S and late S (two biological replicates each) were calculated from the RhIP-ChIP-seq data at 1,000 bp intervals. Left and right panels indicate the correlation coefficients of H2A and H2A.Z data, respectively.

Fig. 5. Identification of important residues for H2A.Z-specific incorporation. (*A*) RhIP-ChIP-seq and ChIP-seq profiles were visualized with the Integrative Genomics Viewer. From top to bottom, profiles of H2A (RhIP-ChIP), H2A.Z (RhIP-ChIP), and H2A.Z (ChIP-seq, GEO:

GSM1003483) are shown with the gene coordination. (*B*) Aggregation plots of the H2A (RhIP-ChIP-seq, left), H2A.Z (RhIP-ChIP-seq, center), and H2A.Z (ChIP-seq, right) localizations around TSSs. (*C*) Amino acid alignments of the H2A.Z M6 region and its counterpart of H2A. The H2A.Z-specific residues of the M6 region, Gly 92, Asp 97, Ser 98, Ile 100, Lys 101, and Ala 102, are highlighted in the H2A.Z-H2B dimer and the H2A.Z nucleosome structure (PDB: 3WA9) in cyan. All residues are located on the surface of the H2A.Z-H2B dimer, but only Gly 92 is visible in the nucleosome structure, since the other residues are located inside the nucleosome. (*D*) Reconstituted H2AZ_M6-H2B, H2A-H2B, and H2A.Z-H2B complexes were analyzed by SDS-16% PAGE with Coomassie Brilliant Blue staining. H2AZ_M6, H2A, and H2A.Z were expressed as N-terminally V5, 3FLAG, and 3HA fused proteins, respectively. Lane 1 indicates the molecular mass markers, and lanes 2-4 indicate the H2A.Z_M6-H2B, H2A-H2B, and H2A.Z-H2B complexes, respectively. (*E*) RhIP-immunostaining images of H2A.Z and H2A.Z_M6. Exogenously added H2A.Z-H2B and H2A.Z_M6-H2B complexes were stained with the anti-V5 or HA antibody. Cells in S phase were monitored with Cy5-dUTP. Bar indicates 10 μm. (*F*) RhIP-immunostaining images of H2A.Z, H2A.Z_M6, and H2A. Exogenously added H2A-H2B complexes were stained with anti-HA, V5, or FLAG antibodies. Bar indicates 10 μm. Histograms along the red line are shown.

Fig. 6. Model of differential histone incorporations into open and closed chromatin. In open chromatin, the H2A-H2B and H2A.X-H2B complexes are incorporated in replication-independent (RI) and replication-coupled (RC) manners, while H2A.Z-H2B is incorporated only in a replication-independent manner. In closed chromatin, new histone depositions of H2A and H2A.X, but not H2A.Z, occur only in a replication-coupled manner. This leads to the global

localizations of H2A-H2B and H2A.X-H2B. It also leads to the specific localization of H2A.Z-H2B, such as its elimination from closed chromatin.

Fig. S1. RhIP assay using recombinant histone chaperones. (*A*) Schematic representation of the RhIP assay. The RhIP assay was performed with H3.1-H4, in the presence of either the cellular extract, or the histone chaperones Nap1 or Asf1. (*B*) Purified human Nap1 and Asf1 were analyzed by SDS-16% PAGE with Coomassie Brilliant Blue staining. Lane 1 indicates the molecular mass markers, and lanes 2 and 3 indicate Nap1 and Asf1, respectively. (*C*) RhIP-immunostaining images of H3.1. The exogenously added H3.1-3HA-H4 complex was stained with an anti-HA antibody. Cells in S phase were monitored with Cy5-dUTP. Bar indicates 10 μm.

Fig. S2. Analysis of histone H2A.X incorporation by the RhIP assay. (*A*) Schematic representation of the RhIP assay, using the reconstituted H2A-H2B and H2A.X-H2B complexes. (*B*) Reconstituted H2A-H2B and H2A.X-H2B complexes were analyzed by SDS-16% PAGE with Coomassie Brilliant Blue staining. 3HA and V5 were fused to the N-termini of H2A and H2A.X, respectively. Lane 1 indicates the molecular mass markers, and lanes 2 and 3 indicate the H2A-H2B and H2A.X-H2B complexes, respectively. (*C*) RhIP-immunostaining images of H2A and H2A.X. Exogenously added H2A-H2B complexes were stained with an anti-HA or V5 antibody. Cells in S phase replication were monitored with Cy5-dUTP. Bar indicates 10 μm.

Fig. S3. Analysis of histone H2A and H2A.Z incorporations in S phase cells with a RhIP-ChIP assay, using synchronized cells. (*A*) Cells were synchronized in early S or late S phase by a

double thymidine block (upper). Cell synchronization was confirmed by the homogeneous replication pattern, using Cy5-dUTP labeling (lower images). (*B*) The immunoprecipitated DNA was analyzed by 1.5% agarose electrophoresis. Upper and lower images were obtained from the same gel. The DNA was visualized with SYBR Gold (upper) and the nascent DNA was visualized by detecting the Cy5 signals (lower). Lane 1 indicates a 100 bp DNA ladder. Lanes 2-7 and 8-13 indicate early S and late S phase samples, respectively. Lanes 2-4 and 8-10 indicate input samples, and lanes 5-7 and 11-13 indicate immunoprecipitated samples, respectively. Each lane indicates a negative control without the reconstituted histone complex (lanes 2, 5, 8, and 11), the samples with 3HA-H2A-H2B (lanes 3, 6, 9, and 12), and the samples with 3HA-H2A.Z-H2B (lanes 4, 7, 10, and 13).

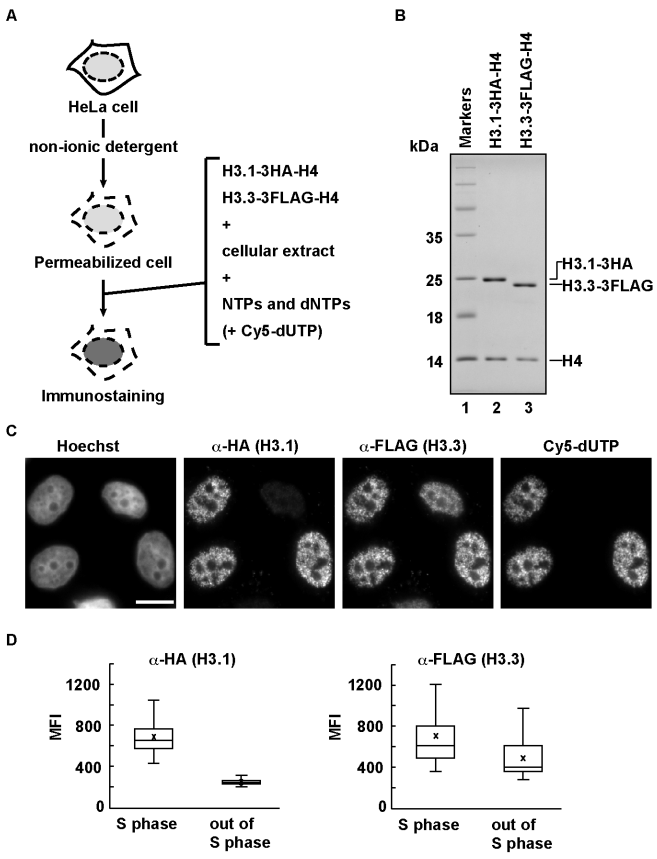
A
HeLa cell
non-ionic detergent
Permeabilized cell
Immunostaining
H3.1-3HA-H4
H3.3-3FLAG-H4
+
cellular extract
+
NTPs and dNTPs
(+ Cy5-dUTP)
B
Markers
H3.1-3HA-H4
H3.3-3FLAG-H4
kDa
35
25
18
14
H3.1-3HA
H3.3-3FLAG
H4
1 2 3
C
Hoechst
α-HA (H3.1)
α-FLAG (H3.3)
Cy5-dUTP
D
α-HA (H3.1)
α-FLAG (H3.3)
MFI
1200
800
400
0
S phase
out of S phase

Figure 1

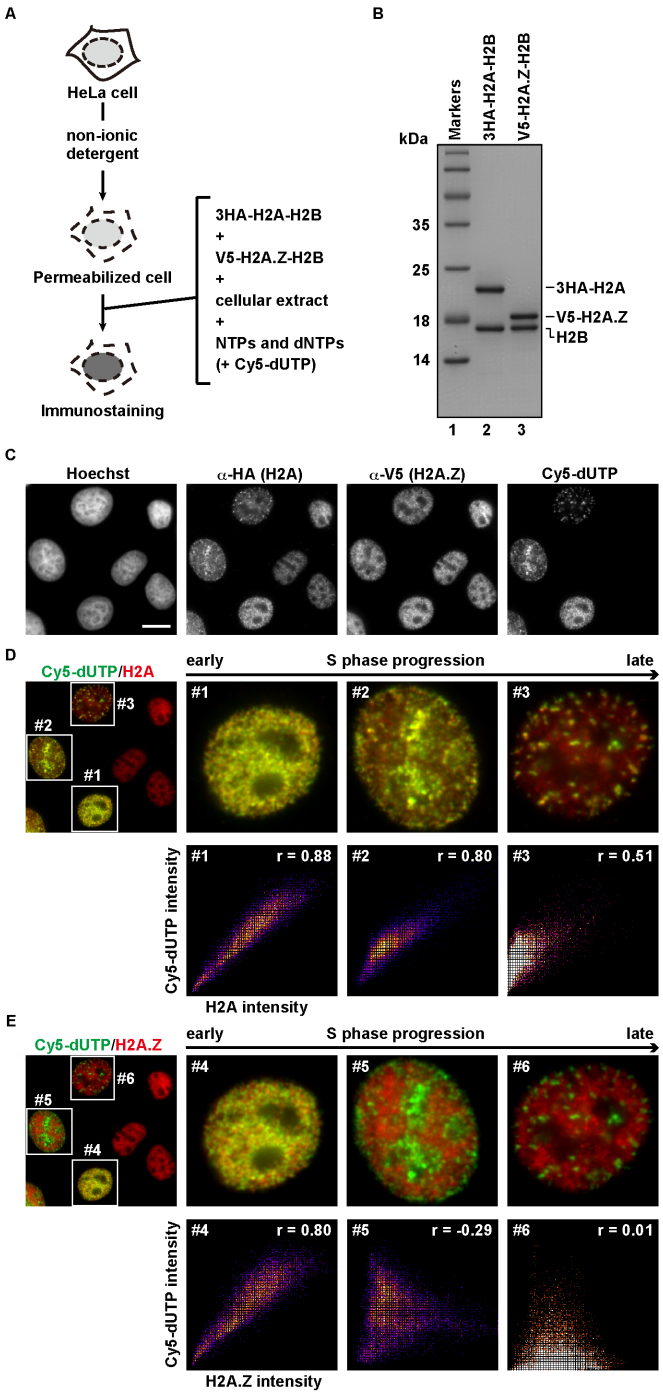
A
HeLa cell
non-ionic detergent
Permeabilized cell
Immunostaining
3HA-H2A-H2B
+
V5-H2A.Z-H2B
+
cellular extract
+
NTPs and dNTPs
(+ Cy5-dUTP)
B
kDa
Markers
3HA-H2A-H2B
V5-H2A.Z-H2B
35
25
18
14
1 2 3
3HA-H2A
V5-H2A.Z
H2B
C
Hoechst
α-HA (H2A)
α-V5 (H2A.Z)
Cy5-dUTP
D
Cy5-dUTP/H2A
early
S phase progression
late
#1
#2
#3
r = 0.88
r = 0.80
r = 0.51
Cy5-dUTP intensity
H2A intensity
E
Cy5-dUTP/H2A.Z
early
S phase progression
late
#4
#5
#6
r = 0.80
r = -0.29
r = 0.01
Cy5-dUTP intensity
H2A.Z intensity

Figure 2

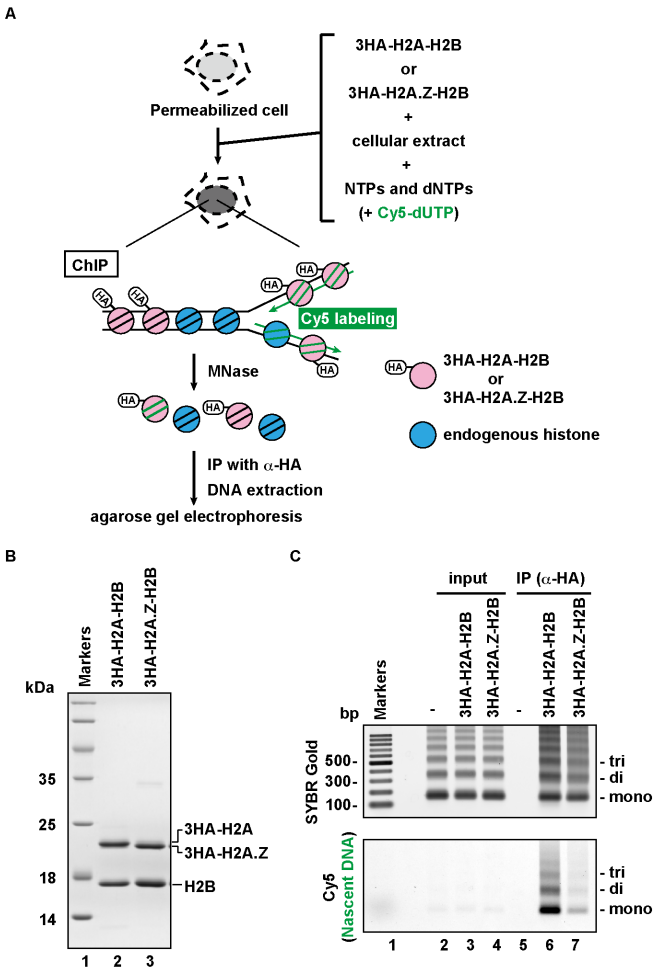
A
Permeabilized cell
3HA-H2A-H2B
or
3HA-H2A.Z-H2B
+
cellular extract
+
NTPs and dNTPs
(+ Cy5-dUTP)
ChIP
Cy5 labeling
MNase
IP with α-HA
DNA extraction
agarose gel electrophoresis
3HA-H2A-H2B
or
3HA-H2A.Z-H2B
endogenous histone
B
kDa
Markers
3HA-H2A-H2B
3HA-H2A.Z-H2B
35
25
18
14
3HA-H2A
3HA-H2A.Z
H2B
1 2 3
C
input
IP (α-HA)
bp
Markers
3HA-H2A-H2B
3HA-H2A.Z-H2B
SYBR Gold
500-
300-
100-
tri
di
mono
Cy5 (Nascent DNA)
1 2 3 4 5 6 7

Figure 3

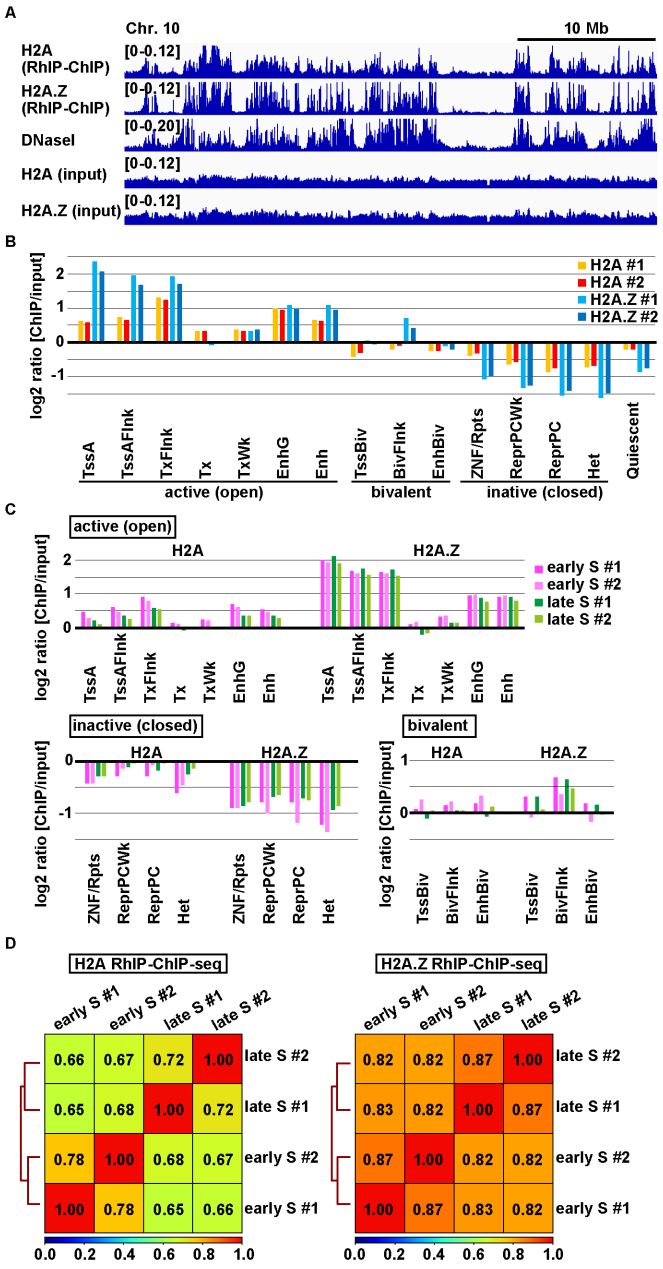
A
Chr. 10
10 Mb
H2A (RhIP-ChIP)
[0-0.12]
H2A.Z (RhIP-ChIP)
[0-0.12]
DNaseI
[0-0.20]
H2A (input)
[0-0.12]
H2A.Z (input)
[0-0.12]
B
log2 ratio [ChIP/input]
H2A #1
H2A #2
H2A.Z #1
H2A.Z #2
TssA
TssAFlnk
TxFlnk
Tx
TxWk
EnhG
Enh
TssBiv
BivFlnk
EnhBiv
ZNF/Rpts
ReprPCWk
ReprPC
Het
Quiescent
active (open)
bivalent
inative (closed)
C
active (open)
inactive (closed)
bivalent
H2A
H2A.Z
early S #1
early S #2
late S #1
late S #2
D
H2A RhIP-ChIP-seq
H2A.Z RhIP-ChIP-seq
0.66 0.67 0.72 1.00
0.65 0.68 1.00 0.72
0.78 1.00 0.68 0.67
1.00 0.78 0.65 0.66
0.82 0.82 0.87 1.00
0.83 0.82 1.00 0.87
0.87 1.00 0.82 0.82
1.00 0.87 0.83 0.82
0.0 0.2 0.4 0.6 0.8 1.0

Figure 4

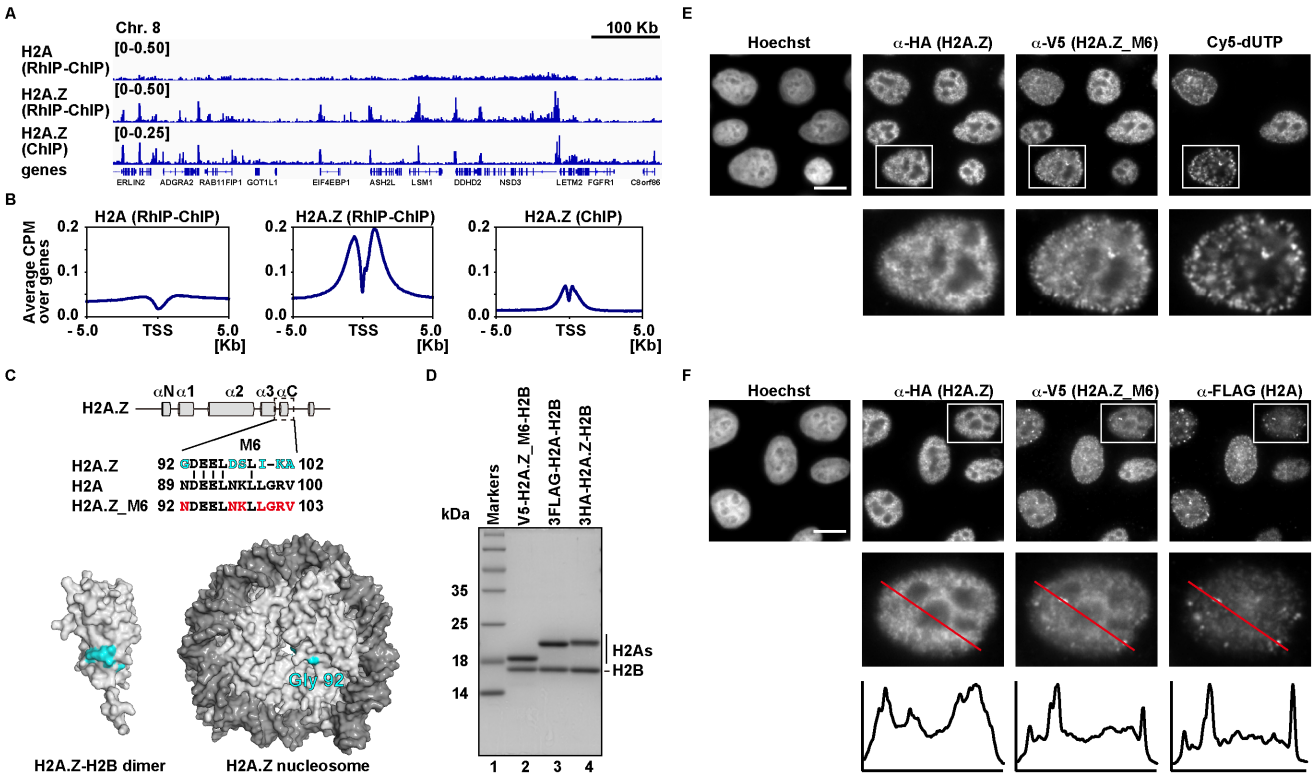
A
Chr. 8
100 Kb
H2A (RhIP-ChIP)
[0-0.50]
H2A.Z (RhIP-ChIP)
[0-0.50]
H2A.Z (ChIP)
[0-0.25]
genes
ERLIN2 ADGRA2 RAB11FIP1 GOT1L1 EIF4EBP1 ASH2L LSM1 DDHD2 NSD3 LETM2 FGFR1 C8orf86
B
H2A (RhIP-ChIP)
H2A.Z (RhIP-ChIP)
H2A.Z (ChIP)
Average CPM over genes
0.2
0.1
0.0
- 5.0
TSS
5.0
[Kb]
C
αN α1 α2 α3 αC
H2A.Z
M6
H2A.Z 92 GDEELDSLI-KA 102
H2A 89 NDEELNKLLGRV 100
H2A.Z_M6 92 NDEELNKLLGRV 103
Gly 92
H2A.Z-H2B dimer
H2A.Z nucleosome
D
kDa
Markers
V5-H2A.Z_M6-H2B
3FLAG-H2A-H2B
3HA-H2A.Z-H2B
35
25
18
14
H2As
H2B
1 2 3 4
E
Hoechst
α-HA (H2A.Z)
α-V5 (H2A.Z_M6)
Cy5-dUTP
F
Hoechst
α-HA (H2A.Z)
α-V5 (H2A.Z_M6)
α-FLAG (H2A)

Figure 5

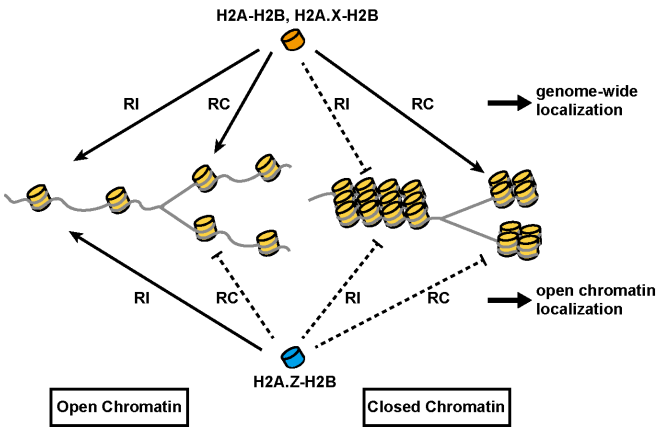
H2A-H2B, H2A.X-H2B
RI
RC
RI
RC
genome-wide localization
RI
RC
RI
RC
open chromatin localization
H2A.Z-H2B
Open Chromatin
Closed Chromatin

Figure 6

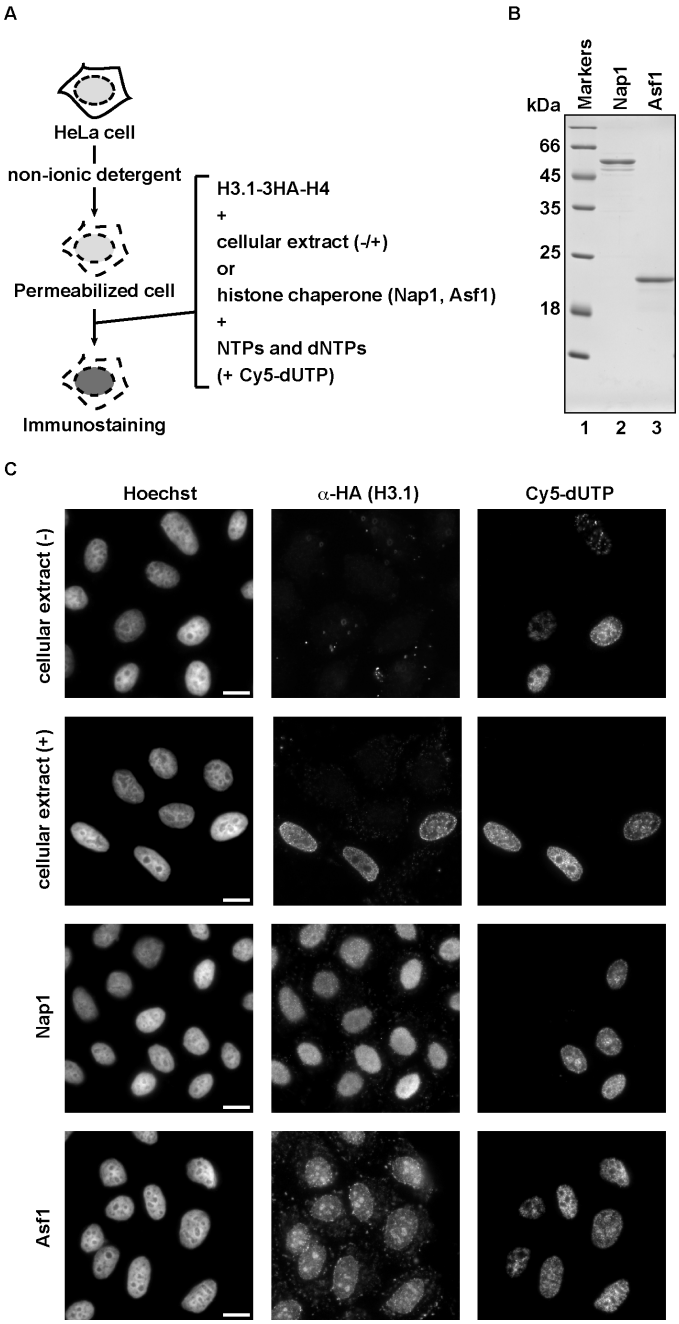
A
HeLa cell
non-ionic detergent
Permeabilized cell
Immunostaining
H3.1-3HA-H4
+
cellular extract (-/+)
or
histone chaperone (Nap1, Asf1)
+
NTPs and dNTPs
(+ Cy5-dUTP)
B
kDa
Markers
Nap1
Asf1
66
45
35
25
18
1
2
3
C
Hoechst
α-HA (H3.1)
Cy5-dUTP
cellular extract (-)
cellular extract (+)
Nap1
Asf1

Figure S1

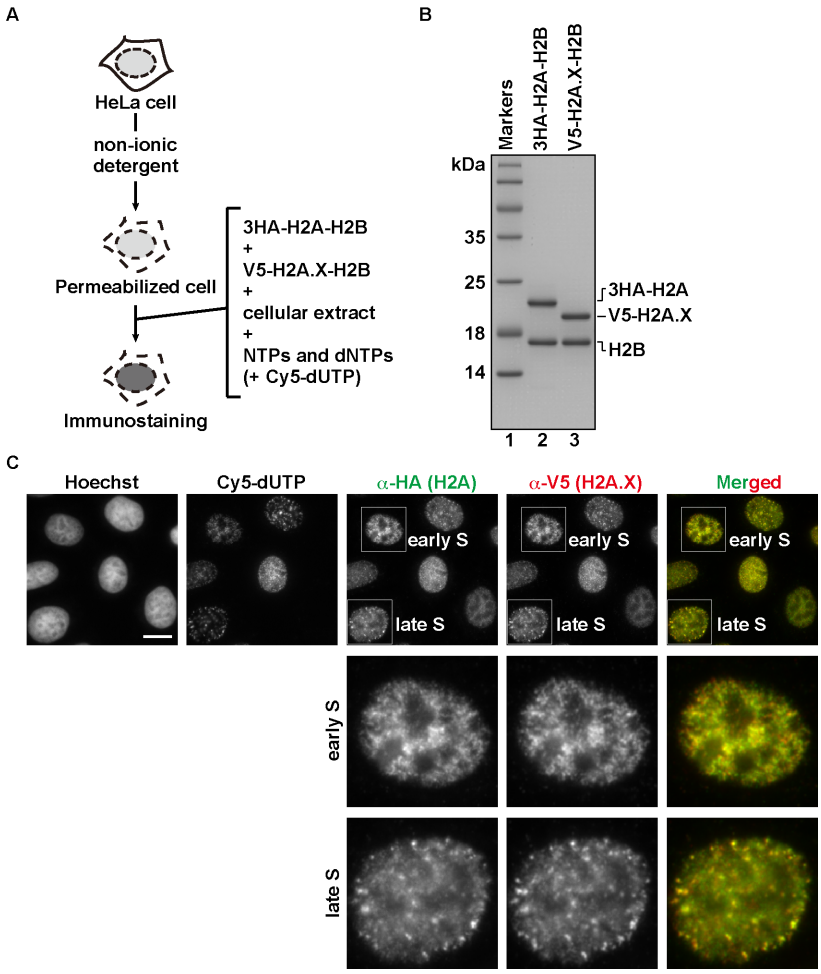
A
HeLa cell
non-ionic detergent
Permeabilized cell
3HA-H2A-H2B
+
V5-H2A.X-H2B
+
cellular extract
+
NTPs and dNTPs
(+ Cy5-dUTP)
Immunostaining
B
Markers
3HA-H2A-H2B
V5-H2A.X-H2B
kDa
35
25
18
14
3HA-H2A
V5-H2A.X
H2B
1 2 3
C
Hoechst
Cy5-dUTP
α-HA (H2A)
α-V5 (H2A.X)
Merged
early S
late S
early S
late S

Figure S2

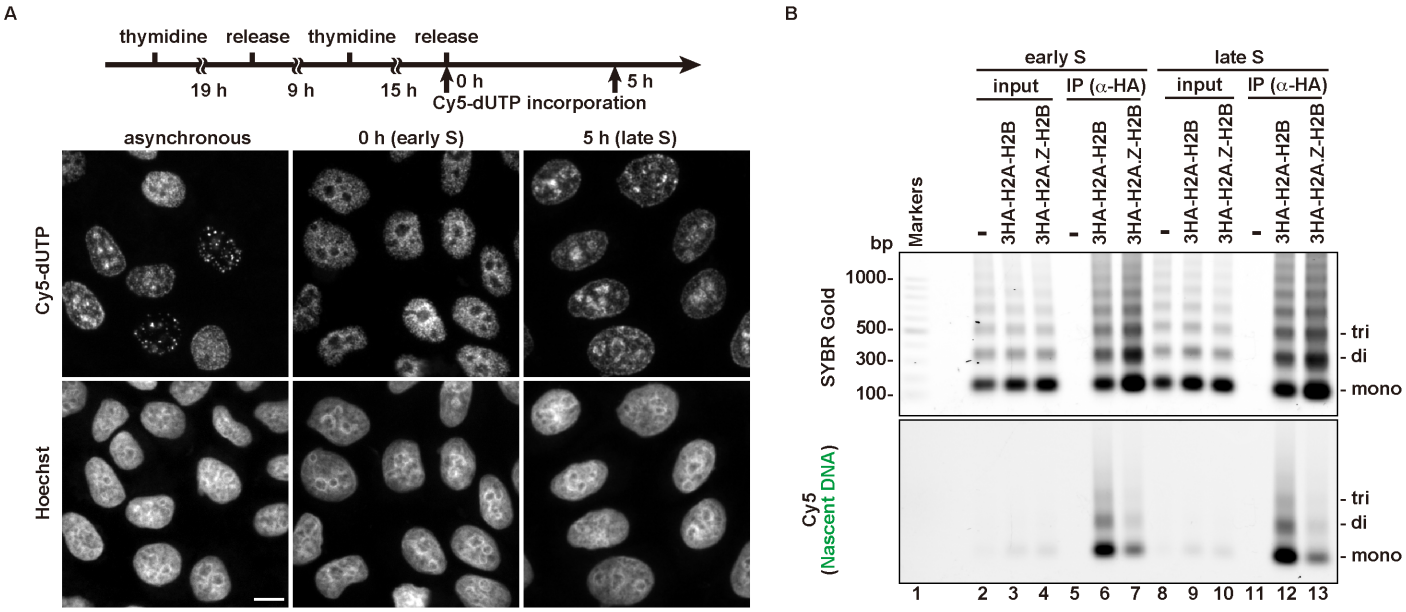
A
thymidine
release
thymidine
release
19 h
9 h
15 h
0 h
5 h
Cy5-dUTP incorporation
asynchronous
0 h (early S)
5 h (late S)
Cy5-dUTP
Hoechst
B
early S
late S
input
IP (α-HA)
input
IP (α-HA)
bp
Markers
-
3HA-H2A-H2B
3HA-H2A.Z-H2B
SYBR Gold
1000-
500-
300-
100-
- tri
- di
- mono
Cy5
(Nascent DNA)
1 2 3 4 5 6 7 8 9 10 11 12 13

Figure S3